

# The Impedance of Spiking Neurons Coupled by Time-Delayed Interaction

Juan Bisquert

The synchronization of populations of interacting spiking neurons is a topic of interest for understanding the operation of the brain and for developing oscillatory-based biomimetic computation. The analysis of the operation of neurons by models such as Hodgkin–Huxley (HH) and FitzHugh–Nagumo (FHN) is based on the electrical and electrochemical concepts. The application of small-signal AC impedance and equivalent circuit methods is a promising tool for the fabrication of artificial neurons and synapses with memristor technologies for neuromorphic computation and sensory-motor autonomous systems. The time domain and impedance spectroscopy analysis of two FHN neurons coupled with a time delay related to the propagation of the action potentials is developed. Depending on the coupling strength and delay time constant, the two neurons become synchronized, in phase opposition for a weak coupling, and in alternating spike packets for the strong interaction. The delayed interaction introduces a new element in the equivalent circuit. A new oscillatory impedance that causes curling of the basic spectral patterns associated with the onset of a limit cycle in the presence of Hopf bifurcations is found. The new pattern is appealing as an experimental tool to determine experimentally the extent of coupling between neurons.

computation for artificial intelligence (AI).<sup>[5,6]</sup> The synchronization of multiple elements is the key feature of oscillator-based computing approaches.<sup>[7]</sup>

The coupling of dynamical neuron models and the analysis of bifurcations of the spiking network has been amply investigated to understand the collective dynamics of neural networks.<sup>[3,8–12]</sup> The simplest model that displays the features of neural interaction consists of two coupled neural systems. The dynamical features resulting from the interaction of the paradigmatic FitzHugh–Nagumo (FHN)<sup>[13,14]</sup> neurons, which is the topic of this paper, have been extensively studied.<sup>[12,15–19]</sup> With the introduction of the time delay interaction the coupled FHN neurons display a transition from the original disordered motions to periodic ones, which is accompanied by complex bifurcation properties.<sup>[20–25]</sup>

Impedance spectroscopy (IS) is a multipurpose characterization technique widely used in materials science and electrochemistry.<sup>[26]</sup> In IS, the system is held at a steady state by the application of constant voltage  $\bar{V}$ . The current  $\bar{I}$  in response to a small periodic perturbation  $\tilde{V}$  of angular frequency  $\omega$  is measured. The resulting linear impedance data is described in terms of an equivalent circuit (EC) model that provides detailed information on the physical processes occurring at different time/frequency scales.


The paradigm of excitability developed by Hodgkin and Huxley<sup>[27]</sup> (HH) emerged from a tradition of analysis of neurons by electrical and electrochemical methods.<sup>[13,28–31]</sup> It is, therefore, interesting to calculate the small perturbation AC impedance properties of neuronal models. Recently, we showed the properties of IS of neuron models like HH<sup>[32]</sup> and FHN.<sup>[33]</sup> We have classified the properties of equivalent circuits and Hopf bifurcations in 2D neuron models.<sup>[34,35]</sup> These insights pave the way to create functional elements for the construction of computational neuronal networks based on memristor elements.<sup>[36,37]</sup> In this work, we show the new aspects of the impedance when two FHN neurons are coupled with time delay.

The structure of the article is as follows. Section 2 revises the impedance model for a single neuron, and Section 3 describes the different schemes of delayed coupling in neuron networks. Section 4 analyzes a specific model in which two FHN neurons are restrained with interactive time delay. Section 5 describes the spiking patterns of the coupled system, and Section 6 shows the associated impedance patterns. We finish with some conclusions.

## 1. Introduction

Synchronous oscillations are a dominant phenomenon in the brain.<sup>[1–4]</sup> The emergence and synchronization of these rhythms are caused by populations of interacting spiking neurons in which the firing of one neuron results in a perturbation of the voltage of a neighbor neuron and displaces the neurons towards synchrony into a coherent oscillation mode. These synchronous oscillations are the origin of brain activity that exists in the absence of external input. Coupled oscillators are also investigated as a biology-inspired practical way to perform

J. Bisquert  
Institute of Advanced Materials (INAM)  
Universitat Jaume I  
12006 Castelló, Spain  
E-mail: bisquert@uji.es

 The ORCID identification number(s) for the author(s) of this article can be found under <https://doi.org/10.1002/pssa.202200064>.

© 2022 The Authors. physica status solidi (a) applications and materials science published by Wiley-VCH GmbH. This is an open access article under the terms of the Creative Commons Attribution-NonCommercial-NoDerivs License, which permits use and distribution in any medium, provided the original work is properly cited, the use is non-commercial and no modifications or adaptations are made.

DOI: 10.1002/pssa.202200064

## 2. Single Neuron Model

We summarize here the main properties of IS of 2D neuron models<sup>[33–35]</sup> before entering a coupled two-neuron system. We consider the transmembrane voltage  $u$ , the total current  $I_{tot}$  and an additional internal state variable  $w$ . A general 2D dynamical model is defined by the following equations<sup>35</sup>

$$\tau_m \frac{du}{dt} = f(u, w, I_{tot}) \quad (1)$$

$$\tau_k \frac{dw}{dt} = g(u, w) \quad (2)$$

Here,  $\tau_m$ ,  $\tau_k$  are the characteristic times of the fast variable  $u$  and the slow variable  $w$ , respectively, accordingly, it is expected the property  $\tau_k \gg \tau_m$  of the excitable neuron membrane.<sup>[38]</sup>  $f$  and  $g$  are in general nonlinear functions that define the properties of the model. A 2D electrical or electrochemical oscillating system contains a negative resistance in the fast variable part  $f$ .<sup>[39]</sup>

The FHN model displays rich bifurcation properties.<sup>[40–43]</sup> It is defined by the following functions<sup>[33]</sup>

$$f = -\frac{u^3}{3} + u - R_I w + R_I I_{tot} \quad (3)$$

$$g = \frac{1}{R_w} u - b w \quad (4)$$

The slow variable  $w$  is an internal recovery current that represents the changes in ion-channel conductance as a function of the voltage. The model introduces a set of specific parameters that establish the possible bifurcations and qualitatively different dynamical evolutions: a channel resistor  $R_I$ , a recovery current resistor  $R_w$ , and a modulation constant  $b$ . We introduce the ratio of timescales and ratio of resistances<sup>[33]</sup>

$$\varepsilon = \frac{\tau_m}{\tau_k} \quad (5)$$

$$r = \frac{R_I}{R_w} \quad (6)$$

According to the dominant channel, the DC resistance is positive as in **Figure 1a**, or it is negative in a saddle feature in **Figure 1b**.

From Equation (1) to (2), one generates the linearized equations that provide impedance spectroscopy criteria for the bifurcation properties. The impedance function is<sup>[35]</sup>

$$Z(s) = [R_b(u)^{-1} + C_m s + (R_a + L_a s)^{-1}]^{-1} \quad (7)$$

The parameters in Equation (7) are

$$C_m = \frac{\tau_m}{R_I} \quad (8)$$

$$R_a = b R_w \quad (9)$$

$$R_b = \left[ \left( \frac{u}{2} \right)^2 - 1 \right]^{-1} R_I \quad (10)$$

$$L_a = \tau_k R_w \quad (11)$$

The EC is shown in **Figure 2a**.  $C_m$  in Equation (8) is the membrane capacitance.  $R_b$  in Equation (10) is the intrinsic resistance of the membrane that contains the negative portion necessary for bifurcations and oscillation.<sup>[33]</sup> The third circuit line in **Figure 2a** is formed by a positive resistance  $R_a$  and the chemical inductor element  $L_a$ .<sup>[34]</sup>

Impedances are usually plotted in the complex plane  $Z = Z' - iZ''$ . The impedance shapes are separated by the Hopf bifurcation voltage  $u_H$ . In the range  $u > u_H$ , the fixed point is a sink and the impedance shows the pattern in **Figure 2b**. The high-frequency arc makes an excursion to the fourth quadrant due to the influence of the inductor. A different spectrum is obtained when the fixed point becomes an unstable source at  $u < u_H$ , **Figure 2c**. The impedance starts with a positive resistance at a low frequency in agreement with the positive slope in **Figure 1a** for  $r/b > 1$ . But at a finite frequency the negative resistance  $R_b$  dominates over  $R_a$  and  $Z$  intersects the negative  $Z'$  axis at a finite frequency. This impedance spectrum with hidden negative resistance,<sup>[44]</sup> **Figure 2c**, is the signature of a stable limit cycle that produces stationary oscillations in the 2D system. The caption of **Figure 2** shows the characteristic frequencies

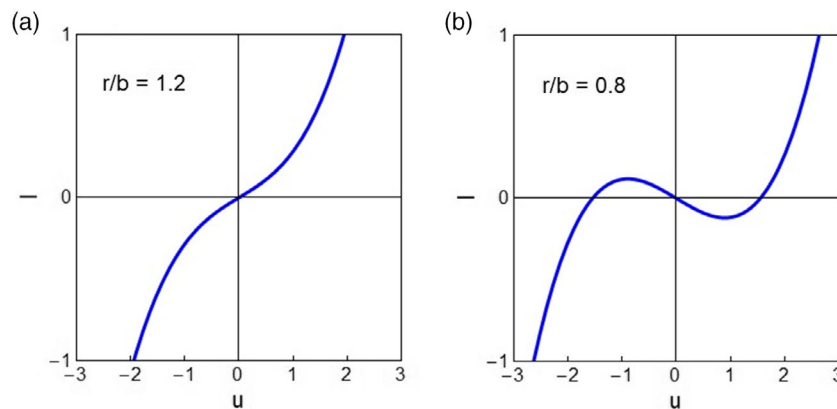


**Figure 1.** Current–voltage stationary curves for  $R_I = 0.5$  and different  $r/b$  as indicated.

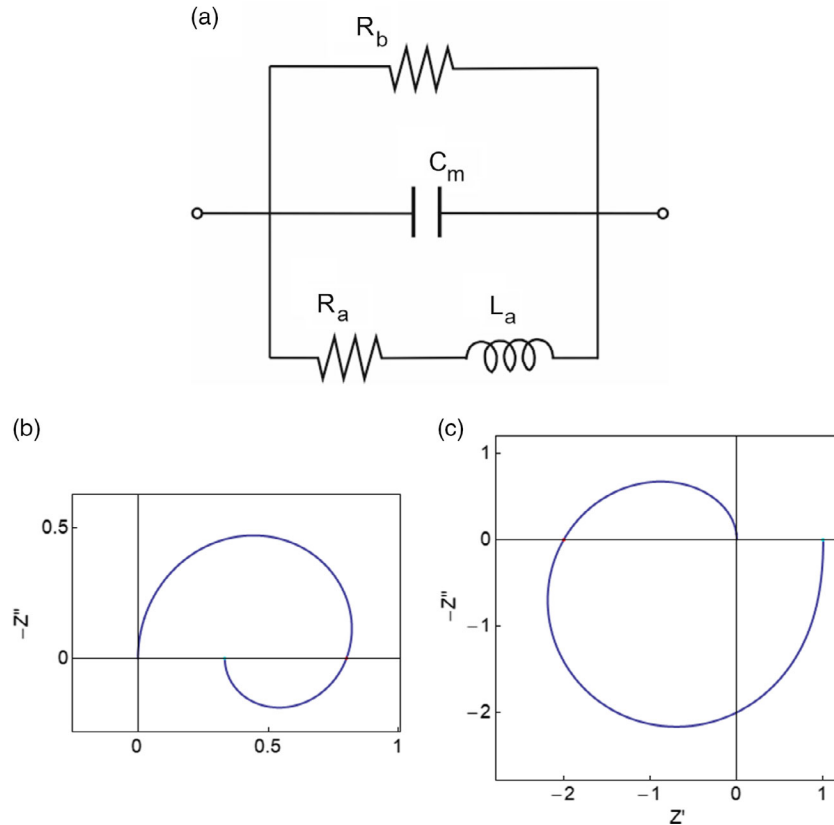


**Figure 2.** a) Equivalent circuit model for the FitzHugh–Nagumo (FHN) model. b,c) Complex plane impedance representation of the spectral patterns. Parameters  $\{R_a, R_b, L_a, C_m\}$ ,  $\{\omega_a, \omega_b, \omega_L, \omega_c, \omega_d, \omega_o, -\omega_L - \omega_b\}$ . b)  $\{\frac{1}{2}, 1, 2, 1\}$   $\{2, 1, \frac{1}{4}, 0.657, \text{Im}, 0.866, -\frac{5}{4}\}$ , c)  $\{\frac{1}{2}, -1, 1, 1\}$   $\{2, -1, \frac{1}{2}, 0.866, 0.5, 0.707, \frac{1}{2}\}$ .

$\{\omega_a, \omega_b, \omega_L, \omega_c, \omega_d, \omega_o, -\omega_L - \omega_b\}$  corresponding to the classification method.<sup>[35]</sup> The Hopf bifurcation occurs when  $\omega_L = -\omega_b$ .

### 3. Coupling of Neurons

Communication between neurons is not instantaneous due to the finite propagating speed in the signal switching and transmission between the neurons. Time delay in the interaction is inevitable in the neural network and should be incorporated into the mathematical model. The analysis of coupled delayed differential equations has been amply studied for the analysis of the stability of neural networks.<sup>[45–47]</sup> An approach to a system of mutually restrained neurons can be established by using a set of elementary neuron dynamical equations as (1–2) and introducing a coupling function  $C$ , as follows<sup>[17,19,23,48–52]</sup>

$$\tau_m \frac{du_i}{dt} = f(u_i, w_i, I_{\text{tot}}) + \sum_{i,j} C_{ij} \quad (12)$$

$$\tau_k \frac{dw_i}{dt} = g(u_i, w_i) \quad (13)$$

where

$$C_{ij}(t) = C_{ij}(u_i(t), u_j(t - \tau_c)) \quad (14)$$

is a coupling function with a delay time  $\tau_c$ . This system of equations allows us to study not only coupled neurons but also the coupling of neuronal subensembles that operate synchronously.<sup>[15]</sup> Different models have been considered for  $C(t)$ , for example, a linear coupling of strength  $\rho_c$ <sup>[15]</sup>

$$C_{ij}(t) = \rho_c [u_j(t - \tau_c) - u_i(t)] \quad (15)$$

A frequently used model is the sigmoid coupling<sup>[20–22,24]</sup>

$$C_j(t) = c_1 \tanh(u_j(t - \tau_c)) \quad (16)$$

The coupling function may include a time-distributed delay via a memory function  $m(t)$ <sup>[50,51]</sup>

$$C_j(t) = c_2 \int_{-\infty}^t m(t-x) u_j(x - \tau_c) dx \quad (17)$$

### 4. Coupled Neurons Model

The dynamical model is based on two FHN neurons coupled by the linear function of Equation (15).<sup>[15,23]</sup> It consists of the following equations<sup>[33]</sup>

$$\tau_m \frac{du_1}{dt} = -\frac{u_1^3}{3} + u_1 + R_I(-w_1 + I_1) + \rho_c[u_2(t - \tau_c) - u_1(t)] \quad (18)$$

$$\tau_k \frac{dw_1}{dt} = \frac{1}{R_w} u_1 - bw_1 \quad (19)$$

$$\tau_m \frac{du_2}{dt} = -\frac{u_2^3}{3} + u_2 + R_I(-w_2 + I_2) + \rho_c[u_1(t - \tau_c) - u_2(t)] \quad (20)$$

$$\tau_k \frac{dw_2}{dt} = \frac{1}{R_w} u_2 - bw_2 \quad (21)$$

The physical variables for each neuron are the membrane voltages  $u_i$  and currents  $I_i$  and the internal recovery currents  $w_i$ . Time is reported in s, voltages in V, current in A, and impedances are given in  $\Omega$ . The independent parameters in the model are the voltage response time  $\tau_m$ , the recovery current response time  $\tau_k$ , channel resistor  $R_I$ , recovery current resistor  $R_w$  and modulation constant  $b$ , delay time  $\tau_c$ , and coupling strength  $\rho_c$ .

We consider that the neurons are connected in series, hence the total voltage  $u$  and current  $I$  satisfy the relations

$$u = u_1 + u_2 \quad (22)$$

$$I = I_1 = I_2 \quad (23)$$

Let us assume that in a steady-state situation (indicated by an overbar) the delay has no effect so that the voltages tend to a unique stationary point.

$$\lim_{t \rightarrow \infty} [u_2(t - \tau_c) - u_1(t)] = 0 \quad (24)$$

Then the model is symmetric, hence  $\bar{u}_i = \bar{u}_1/2 = \bar{u}_2/2$ . The stationary current-voltage ( $I - u$ ) is independent of the coupling parameters, and it has the following expression

$$\bar{I} = \frac{1}{2R_I} \left[ \frac{1}{12} \bar{u}^3 + \left( \frac{r}{b} - 1 \right) \bar{u} \right] \quad (25)$$

The possible forms are shown in Figure 1. The DC resistance is

$$R_{dc}^{-1} = \frac{dI}{du} = \frac{1}{2R_I} \left[ \frac{\bar{u}^2}{4} + \frac{r}{b} - 1 \right] \quad (26)$$

The coupling resistance is

$$R_\rho = \frac{R_I}{\rho_c} \quad (27)$$

To derive the response to a small perturbation, we develop linearly Equation (18)–(21), with small quantities indicated by a tilde. To obtain the AC impedance, we take the standard method of Laplace transform,  $d/dt \rightarrow s$ , where  $s = i\omega$ . Consider the delay differential equation

$$\frac{dx}{dt} = f(x(t), x(t - \tau)) \quad (28)$$

$$x(t) = g(t), t \in [-\tau, 0] \quad (29)$$

$$x(t) = x_0, t = 0 \quad (30)$$

The Laplace transform of the delayed function is

$$\begin{aligned} L[x(t - \tau)] &= e^{-s\tau} \int_{-\tau}^0 e^{-st} g(t) dt + e^{-s\tau} \int_0^\infty e^{-st} x(t) dt \\ &= e^{-s\tau} G(s) + e^{-s\tau} X(s) \end{aligned} \quad (31)$$

In the oscillatory regime of ac impedance we neglect the term of the initial function  $G(s)$  in the last line of (31).

From Equation (18)–(21) we arrive at the system

$$C_m s \tilde{u}_1 = -\left( \frac{1}{R_b} + \frac{1}{R_\rho} \right) \tilde{u}_1 + \frac{1}{R_\rho} e^{-s\tau_c} \tilde{u}_2 - \tilde{w}_1 + \bar{I} \quad (32)$$

$$s \tilde{w}_1 = \frac{1}{L_a} \tilde{u}_1 - \frac{b}{\tau_k} \tilde{w}_1 \quad (33)$$

$$C_m s \tilde{u}_2 = -\left( \frac{1}{R_b} + \frac{1}{R_\rho} \right) \tilde{u}_2 + \frac{1}{R} e^{-s\tau_c} \tilde{u}_1 - \tilde{w}_2 + \bar{I} \quad (34)$$

$$s \tilde{w}_2 = \frac{1}{L_a} \tilde{u}_2 - \frac{b}{\tau_k} \tilde{w}_2 \quad (35)$$

The characteristic equation of the linearized system is

$$\begin{pmatrix} -\left( \frac{u^2}{4} - 1 + \rho_c \right) - \lambda & -R_I & \rho_c e^{-\lambda \tau_c} & 0 \\ \frac{\epsilon r}{R_I} & -b\epsilon - \lambda & 0 & 0 \\ \rho_c e^{-\lambda \tau_c} & 0 & -\left( \frac{u^2}{4} - 1 + \rho_c \right) - \lambda & -R_I \\ 0 & 0 & \frac{\epsilon r}{R_I} & -b\epsilon - \lambda \end{pmatrix} = 0 \quad (36)$$

That is

$$\begin{aligned} &\left[ \lambda^2 + \left( \frac{u^2}{4} - 1 + \rho_c + b\epsilon \right) \lambda + b\epsilon \left( \frac{u^2}{4} - 1 + \rho_c + \frac{r}{b} \right) \right]^2 \\ &- [\rho_c e^{-\lambda \tau_c} (b\epsilon + \lambda)]^2 = 0 \end{aligned} \quad (37)$$

where  $\lambda$  is in units  $\tau_m^{-1}$ . Equation (37) is a transcendental equation that determines the bifurcation properties of the system.<sup>[20–25]</sup>

We discuss the situation with no delay  $\tau_c = 0$ . Taking a square root in Equation (37), we obtain

$$\lambda^2 - T_\lambda \lambda + \Delta = 0 \quad (38)$$

Hence

$$\lambda_i = \frac{1}{2} \left( T_\lambda \pm \sqrt{T_\lambda^2 - 4\Delta} \right) \quad (39)$$

A parameter  $t_b = 1 \pm 1$  provides two types of conjugated roots, where the first case  $t_b = 0$  corresponds to a duplication of the

interaction-free system that has been explained before<sup>[33]</sup> while  $t_b = 2$  is due to the instantaneous coupling. We have

$$T_\lambda = 1 - \frac{u^2}{4} - b\epsilon - t_b\rho_c \quad (40)$$

$$\Delta = b\epsilon\left(\frac{u^2}{4} - 1 + \frac{r}{b} + t_b\rho_c\right) = b\epsilon R_I\left(\frac{2}{R_{dc}} + \frac{t_b}{R_\rho}\right) \quad (41)$$

$$T_\lambda^2 - 4\Delta = \left(1 - \frac{u^2}{4} + b\epsilon - t_b\rho_c\right)^2 - 4r\epsilon \quad (42)$$

We obtain the following characteristics. 1)  $\Delta < 0$  corresponds to real eigenvalues  $\lambda_{1,2}$  with opposite sign. For  $t_b = 0$ , this is the region of negative  $R_{dc}$ , resulting in three fixed points (a saddle and two sinks) that occur when  $r/b < 1$ , Figure 1b. 2) In contrast,  $\Delta > 0$  and  $t_b = 0$  correspond to a single-valued  $I - u$  curve, Figure 1a. Here, the stability of the fixed point  $I(u)$  is determined by  $T_\lambda < 0$ . At  $T_\lambda = 0$  is a Hopf bifurcation. When  $T_\lambda > 0$  and  $T_\lambda^2 - 4\Delta < 0$ , the fixed point becomes an unstable source with a pair of complex conjugate values in Equation (33). Hence the two-neuron system contains Hopf bifurcations without interactions, which impedance spectra have been described before.<sup>44</sup> 3) When  $t_b = 2$  a new bifurcation point is added due to  $\rho_c$ ,

according to Equations (40) and (41). 4) The previous results are for  $\tau_c = 0$ . The delay  $\tau_c$  is yet an additional bifurcation parameter that has been amply studied in the literature.<sup>[20–25]</sup>

## 5. Spiking Patterns

We analyze the following situation of the positive DC resistance corresponding to  $r/b > 1$ , Figure 1a. In **Figure 3, 4 and 5**, we show the dynamical patterns with progressive complexity. Here we discuss the time domain response and the impedance patterns will be analyzed in Section 6. A Mathematica program for calculations of the model is provided in Supporting Information.

Figure 3 shows the uncoupled system that has two types of behaviors according to the Hopf bifurcation voltage  $u_H$ .<sup>[33]</sup> For  $u > u_H$ , the voltages of the two neurons tend to the fixed point corresponding to the  $I - u$  characteristic, Figure 3a, and for  $u < u_H$  both neurons effect stable limit cycle oscillations, Figure 3b.

When we set the coupling parameter  $\rho_c$  (without delay,  $\tau_c = 0$ ) in Figure 4a, the neurons become fully synchronized. Introducing a short value of delay time constant  $\tau_c = \tau_k$ , Figure 4b, the neurons oscillate in antiphase. For a longer  $\tau_c$ , an alternating rhythm comprising a few oscillations alternated with a rest period appears, Figure 4c, and for a very long

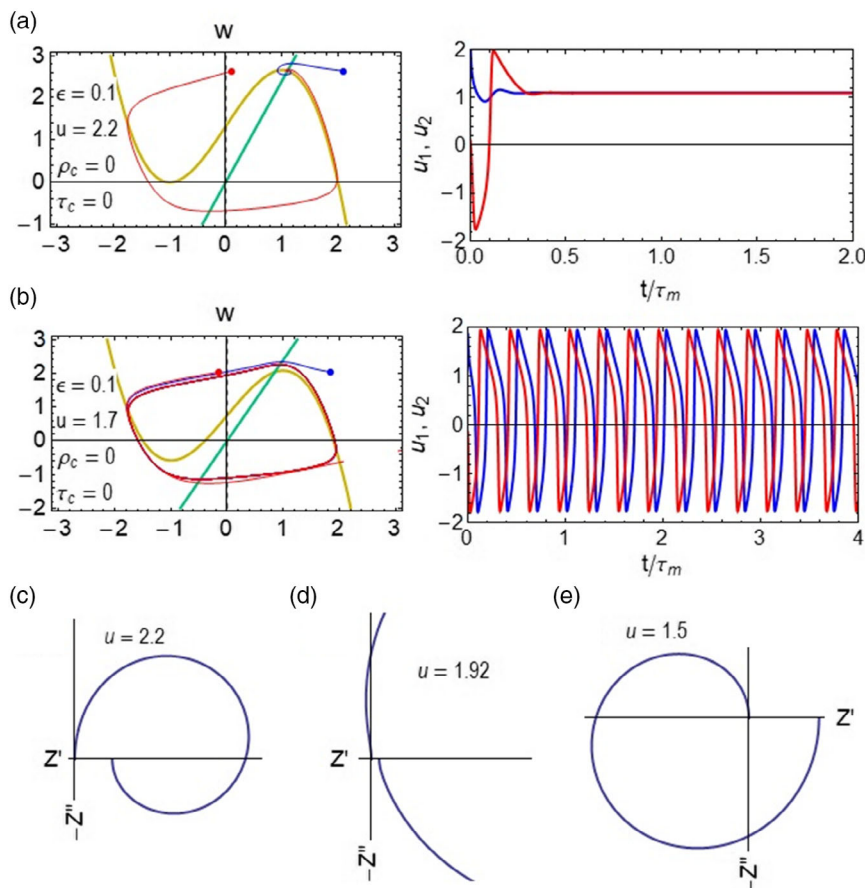


**Figure 3.** The neurons patterns for noninteraction case. a,b) The first column shows the trajectories in the phase plane, second is the voltage dependence on time for the two neurons. c,d,e) Impedance spectra patterns.  $R_I = 0.5$ ,  $b = 1$ ,  $r = 1.2$ ,  $\tau_m = 10^{-2}$ , initial conditions  $u_{10} = u_{app}/2 + 1$ ,  $u_{20} = u_{app}/2 - 1$ ,  $w_{01} = w_{02} = 2$ , and the rest of the parameters as indicated. Hopf bifurcation voltage for no interaction case:  $u_H = 1.8974$ .



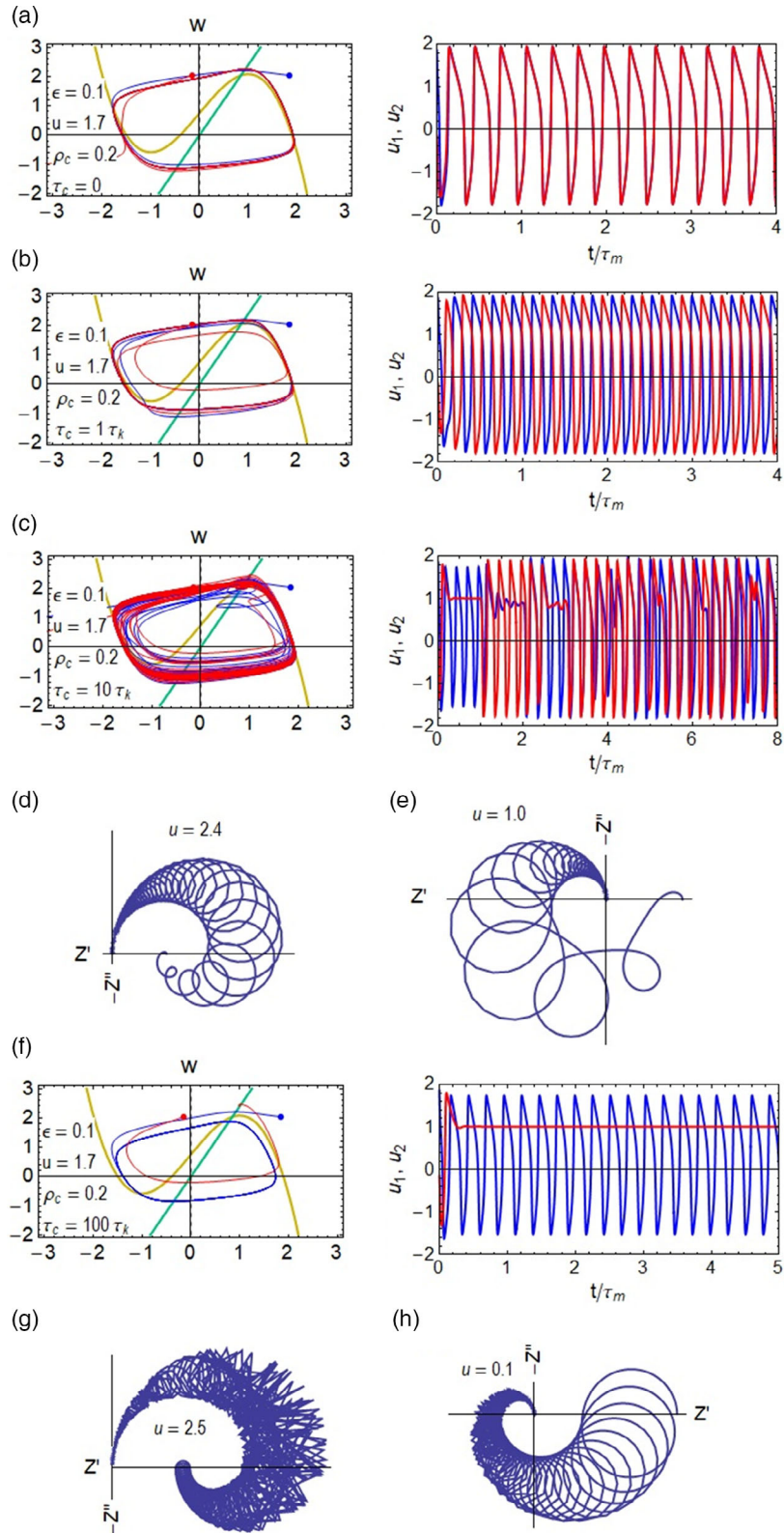


**Figure 4.** Two coupled neuron neurons patterns. a,b,c,f) The first column shows the trajectories in the phase plane, second is the voltage dependence on time for the two neurons, and d,e,g,h) the impedance spectra patterns.  $R_l = 0.5$ ,  $b = 1$ ,  $r = 1.2$ ,  $\tau_m = 10^{-2}$ , initial conditions  $u_{10} = u_{app}/2 + 1$ ,  $u_{20} = u_{app}/2 - 1$ ,  $w_{01} = w_{02} = 2$ , and the rest of the parameters as indicated. Hopf bifurcation voltage for no interaction case:  $u_H = 1.8974, 1.4142$ .

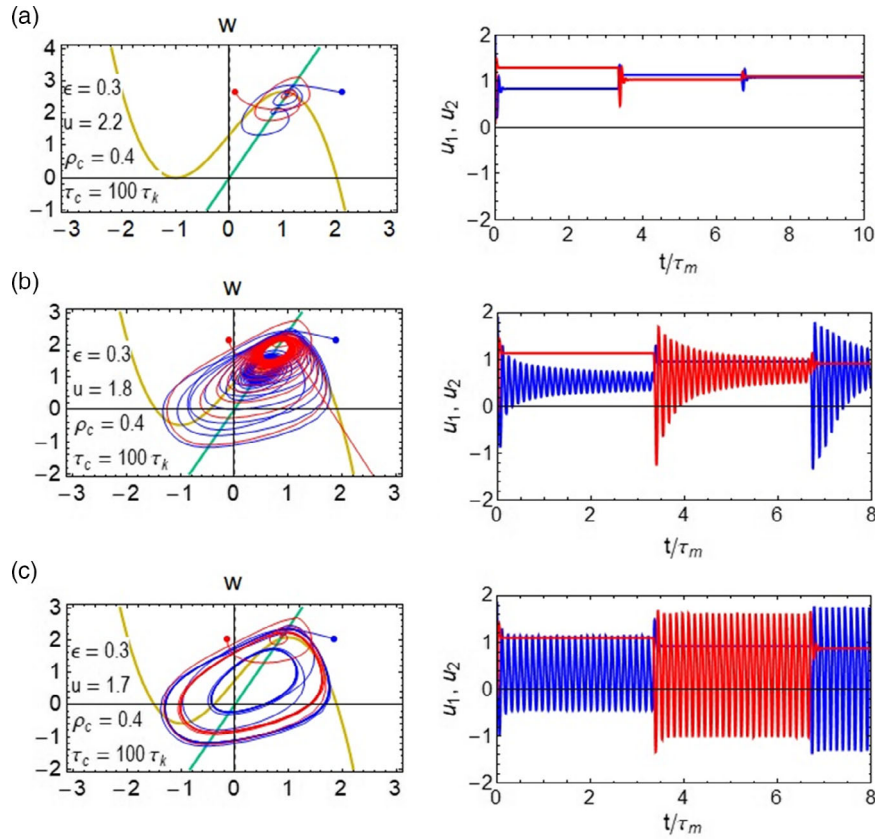


**Figure 5.** Oscillatory patterns in the coupling of two neurons. The first column shows the trajectories in the phase plane, second is the voltage dependence on time for the two neurons.  $R_l = 0.5$ ,  $b = 1$ ,  $r = 1.2$ ,  $\tau_m = 10^{-2}$ , initial conditions  $u_{10} = u_{app}/2 + 1$ ,  $u_{20} = u_{app}/2 - 1$ ,  $w_{01} = w_{02} = 2$ , and the rest of the parameters as indicated. Hopf bifurcation voltage for no interaction case:  $u_H = 1.6733$ .

$\tau_c \gg \tau_k$  one molecule falls to a steady voltage and the other one oscillates, Figure 4f.

In Figure 5, we introduce a stronger coupling  $\rho_c$ . At high voltage in Figure 5a, the two neurons tend to two different coupled fixed points that add up to the applied voltage, in long steps. As we reduce the voltage in Figure 5b approaching the Hopf bifurcation, the neurons alternate in attaining a fixed value with a damped oscillation. For a small voltage in Figure 5c, the alternation of limit cycles as in Figure 4c occurs.

## 6. Impedance Patterns

To obtain the impedance  $Z = \tilde{u}/\tilde{I}$ , we solve the system of Equation (32)–(35). The result is

$$(s) = 2[R_b(u)^{-1} + C_m s + (R_a + L_a s)^{-1} + Z_\rho^{-1}]^{-1} \quad (43)$$

$$Z_\rho(s) = \frac{R_\rho}{1 - e^{-s\tau_c}} \quad (44)$$

The EC corresponding to Equation (43) contains four parallel branches as indicated in Figure 6a. The upper three branches correspond to the single neuron impedance EC model as described before in Figure 2a. In the interaction-free system,

we have the patterns discussed before in Figure 2, see Figure 3c,e. Approaching the bifurcation, Figure 3d, the positive arc takes a shape close to a circle and the impedance crosses to the negative  $Z'$  at high frequency but there is not yet a negative real impedance, that occurs after the Hopf bifurcation in Figure 3e.

The last branch of Figure 6a is the contribution produced by the delayed coupling, which consists of the impedance  $Z_\rho$  in Equation (44). To the best of our knowledge, this impedance function is not previously reported. We can write it as

$$Z_\rho(\omega) = \frac{R_\rho}{2} \left( 1 - i \frac{\sin(\omega\tau_c)}{1 - \cos(\omega\tau_c)} \right) \quad (45)$$

The real part is a constant and the imaginary part is highly oscillatory, with poles at the frequencies

$$\omega_n = \frac{2n\pi}{\tau_c} \quad (46)$$

The function is shown in Figure 6b,c. We can write the admittance as

$$\frac{1}{Z_\rho} = \frac{1}{R_\rho} [1 - \cos(\omega\tau_c) - i \sin(\omega\tau_c)] \quad (47)$$

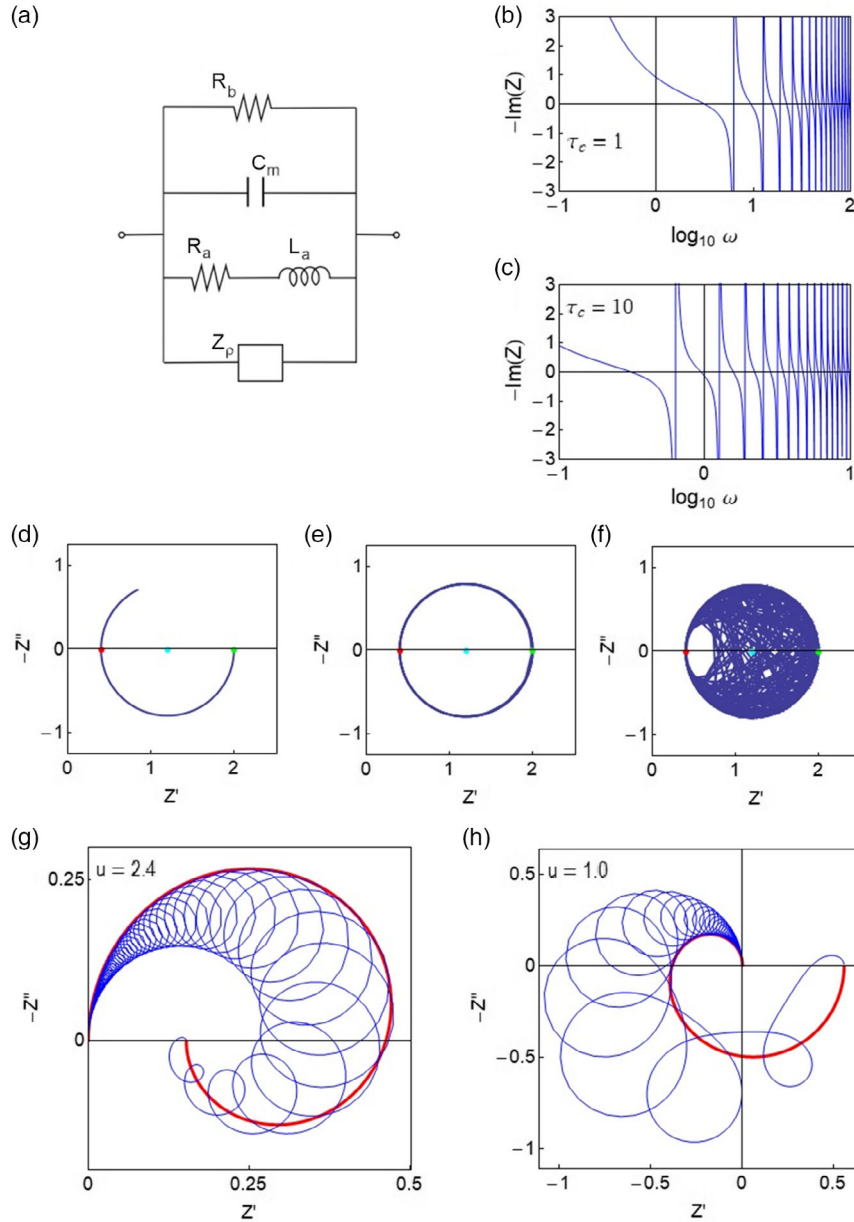


**Figure 6.** a) Equivalent circuit of the coupled neuron system. b,c) Representation of the imaginary part of the impedance  $Z_p$  as a function of frequency. d,e,f) Complex plane representation of the impedance  $Z_p(\omega)$  with a parallel resistance  $R_p = 2$  for  $R_p = 1$ ,  $\tau_c = 1$  and the frequency interval  $\omega = (0.1, f_1) \times 2\pi$ , for: d)  $f_1 = 1$ , d)  $f_1 = 10$ , d)  $f_1 = 100$ . Points indicate the circle parameters: Red  $Z_a$ , cyan  $Z_c$ , green  $Z_b$ . g,h) Representation of the total impedance for  $R_l = 0.5$ ,  $b = 1$ ,  $r = 1.2$ ,  $\tau_m = 10^{-2}$ ,  $\epsilon = 0.1$ ,  $\rho_c = 0$ ,  $\tau_c = 0$  (red line) and  $\rho_c = 0.2$ ,  $\tau_c = 10\tau_k$  (blue line).

If we add a parallel resistor  $R_1$  then the impedance traces a circle centered in the point of the real axis

$$Z_a = \frac{R_p}{2 + \frac{R_p}{R_1}} \quad (49)$$

$$Z_c = \frac{R_p + R_1}{2 + \frac{R_p}{R_1}} \quad (48)$$

$$Z_b = R_1 \quad (50)$$

The minimum and maximum values in the  $Z'$  axis are given by

Figure 6d–f shows the impedance  $Z_p(\omega)$  with a parallel resistance for different ranges of frequency. Initially, it is a neat circumference but when  $\omega \gg \tau_c$  the oscillatory function fills the space and forms a circle.



We can now turn to the analysis of impedance patterns of the full model of Equation (43) and Figure 6a. In Figure 4d, e, the delayed coupling of the neurons is active. By Equation (43), the original hook impedance of Figure 2b is combined in parallel with the oscillatory  $Z_p$ . The resulting impedance in Figure 4d is coiled around the basic pattern, tracing the shape of an ammonite. The same occurs for the impedance shape for a voltage below the Hopf bifurcation in Figure 4e. For a longer coupling time, the coiled regions become denser, Figure 4g,h. Figure 6g,h shows the curling of the impedance when the interaction is added to the coupling-free system. It occurs inwards for  $u > u_H$ , and outwards for  $u < u_H$ .

## 7. Conclusion

We have discussed the dynamical regimes of two identical neurons coupled with time delay, from the point of view of electrical models. Based on previous work that describes the impedance spectroscopy of a single 2D model neuron, here we obtain the spiking patterns and impedance response of the interacting system. For a weak interaction, the spikes become simply dephased, but for stronger interactions trains of spikes appear, and the excitation is alternated between the two neurons. In the coupled system, the basic impedance patterns of the single neuron obtain a curling form depending on the relation of the delay time to the intrinsic time of the neurons. In principle, the new types of spectra appear suitable for a direct experimental identification of coupled neuron spiking by impedance spectroscopy. The analysis of larger networks which is an important objective of the work appears challenging. It will be necessary to separate the effects of delay and internal excitation in the impedance spectra to detect new bifurcations and ensemble synchronization.

## Supporting Information

Supporting Information is available from the Wiley Online Library or from the author.

## Conflict of Interest

The author declares no conflict of interest.

## Data Availability Statement

The data that support the findings of this study are available from the corresponding author upon reasonable request.

## Keywords

artificial neurons, impedance spectroscopy, memristors, neuromorphic computation, synapses

Received: January 31, 2022

Revised: March 18, 2022

Published online:

- [1] G. Buzsáki, N. Logothetis, W. Singer, *Neuron* **2013**, *80*, 751.
- [2] W. Singer, *Eur. J. Neurosci.* **2018**, *48*, 2389.
- [3] B. Ermentrout, T.-W. Ko, *Philos. Trans. Roy. Soc. A: Math. Phys. Eng. Sci.* **2009**, *367*, 1097.
- [4] R. M. Smeal, G. B. Ermentrout, J. A. White, *Philos. Trans. Roy. Soc. B: Biol. Sci.* **2010**, *365*, 2407.
- [5] G. Csaba, W. Porod, *Appl. Phys. Rev.* **2020**, *7*, 011302.
- [6] S. Muroga, K. Takashima, *IRE Trans. Electron. Comput.* **1959**, *EC-8*, 308.
- [7] A. Mallick, M. K. Bashar, D. S. Truesdell, B. H. Calhoun, S. Joshi, N. Shukla, *Nat. Commun.* **2020**, *11*, 4689.
- [8] X.-J. Wang, G. Buzsáki, *J. Neurosci.* **1996**, *16*, 6402.
- [9] X. Liao, S. Li, G. Chen, *Neural Networks* **2004**, *17*, 545.
- [10] B. Lindner, J. García-Ojalvo, A. Neiman, L. Schimansky-Geier, *Phys. Rep.* **2004**, *392*, 321.
- [11] F. Lagzi, F. M. Atay, S. Rotter, *Sci. Rep.* **2019**, *9*, 11397.
- [12] A. Hjelmfelt, J. Ross, *Proc. Natl. Acad. Sci.* **1994**, *91*, 63.
- [13] M. E. Yamakou, T. D. Tran, L. H. Duc, J. Jost, *J. Math. Biol.* **2019**, *79*, 509.
- [14] R. FitzHugh, *Biophys. J.* **1961**, *1*, 445.
- [15] E. Schöll, G. Hiller, P. Hövel, M. A. Dahlem, *Philos. Trans. Roy. Soc. A: Math. Phys. Eng. Sci.* **2009**, *367*, 1079.
- [16] P. McGraw, M. Menzinger, *Phys. Rev. E* **2011**, *83*, 037102.
- [17] Z. Wang, S. A. Symmetry Campbell, *Chaos* **2017**, *27*, 114316.
- [18] B. Zhen, Z. Song, *Neural Plast.* **2021**, *2021*, 6657835.
- [19] L. Santana, R. M. da Silva, H. A. Albuquerque, C. Manchein, *Chaos* **2021**, *31*, 053107.
- [20] Q. Wang, Q. Lu, G. Chen, Z. Feng, L. Duan, *Chaos Solit. Fract.* **2009**, *39*, 918.
- [21] D. Fan, L. Hong, *Commun. Nonlin. Sci. Numer. Simul.* **2010**, *15*, 1873.
- [22] B. Zhen, J. Xu, *Neurocomput.* **2010**, *73*, 874.
- [23] Y. Song, J. Xu, *IEEE Trans. Neural Networks Learn. Syst.* **2012**, *23*, 1659.
- [24] N. Farajzadeh Tehrani, M. Razvan, *Math. Biosci.* **2015**, *270*, 41.
- [25] M. M. Ibrahim, M. A. Kamran, M. M. N. Mannan, I. H. Jung, S. Kim, *Sci. Rep.* **2021**, *11*, 3884.
- [26] A. Lasia, in *Electrochemical Impedance Spectroscopy And Its Applications*, Springer, New York **2014**.
- [27] A. L. Hodgkin, A. F. Huxley, *J. Physiol.* **1952**, *117*, 500.
- [28] L. Lapicque, *J. Physiol. Pathol. Gen.* **1907**, *9*, 620.
- [29] L. Hermann, *Pfluegers Arch.* **1905**, *95*, 95.
- [30] M. Philippson, *Bull. Acad. R. Belg. Clin. Sci.* **1921**, *7*, 387.
- [31] B. S. Pallotta, P. K. Wagoner, *Physiol. Rev.* **1992**, *72*, S49.
- [32] A. Bou, J. Bisquert, *J. Phys. Chem. B* **2021**, *125*, 9934.
- [33] J. Bisquert, *J. Phys. Chem. Lett.* **2021**, *12*, 11005.
- [34] J. Bisquert, A. Guerrero, *J. Am. Chem. Soc.* **2022**, <https://doi.org/10.1021/jacs.1022c00777>.
- [35] J. Bisquert, *Appl. Phys. Rev.* **2022**, *9*, 011318.
- [36] B. Linares-Barranco, *Nat. Electron.* **2018**, *1*, 100.
- [37] G. Indiveri, B. Linares-Barranco, R. Legenstein, G. Deligeorgis, T. Prodromakis, *Nanotechnology* **2013**, *24*, 384010.
- [38] C. Kuehn, in *Multiple Time Scale Dynamics*, Springer, New York **2015**.
- [39] K. Krischer, K. in *Advances In Electrochemical Science And Engineering*, Vol. 8, (Eds: R. C. Alkire, D.M. Kolb), Wiley, Hoboken, NJ **2002**; pp 89–208.
- [40] E. M. Izhikevich, *Dynamical Systems In Neuroscience*, MIT Press, Cambridge, MA **2007**.
- [41] C. Ročsoreanu, A. Georgescu, N. Giurgițeanu, *The FitzHugh-Nagumo Model: Bifurcation And Dynamics*, Kluwer Academic Publishers, Amsterdam **2000**.
- [42] T. Kostova, R. Ravindran, M. Schonbek, *Int. J. Bifurcat. Chaos* **2004**, *14*, 913.
- [43] D. Armbruster, *Nonlin. Dynamics* **1997**, *2*, 89.
- [44] M. T. M. Koper, J. H. Sluyters, *J. Electroanal. Chem.* **1994**, *371*, 149.

- [45] N. C. Majee, A. B. Roy, *Appl. Math. Modell.* **1997**, 21, 673.  
[46] L. Olien, J. Bélair, *Phys. D: Nonlin. Phenom.* **1997**, 102, 349.  
[47] J. Wei, S. Ruan, *Phys. D: Nonlin. Phenom.* **1999**, 130, 255.  
[48] Z. Cheng, J. Cao, *Nonlin. Dynam.* **2006**, 46, 363.  
[49] M. Xiao, W. X. Zheng, J. Cao, *Neurocomputing* **2013**, 99, 206.  
[50] H. Wang, J. Wang, *Math. Methods Appl. Sci.* **2015**, 38, 4967.  
[51] C. Xu, Q. Zhang, Y. Wu, *Cognit. Comput.* **2016**, 8, 1103.  
[52] Y. Wang, Z. Cheng, in *IEEE 8th Data Driven Control and Learning Systems Conf.*, IEEE, Piscataway, NJ **2019**.